Plasmon-enhanced electroluminescence of a single molecule: A theoretical study

Yuan Zhang,[1] Yaroslav Zelinskyy,[1,2] and Volkhard May[1,*]

[1]*Institut für Physik, Humboldt–Universität zu Berlin, Newtonstraße 15, D-12489 Berlin, Germany*
[2]*Bogolyubov Institute for Theoretical Physics, National Academy of Sciences of Ukraine, Metrologichna street 14-b, UA-03143 Kiev, Ukraine*

Photoemission of a molecular junction which is sandwiched between two Au nanospheres is studied theoretically. The Au spheres form a nanoresonator in which plasmon hybrid levels may strongly couple to the radiative transition in the molecular junction. To describe the resulting enhanced electroluminescence, a density matrix approach is introduced which is valid for the regime of sequential charge transmission through the molecule. The simulations account for energy exchange coupling between the molecule and the nanoresonator plasmon excitations, for nonradiative and radiative decay and for vibrational relaxation. Frequency-resolved photon emission spectra are also computed. The effects of varied molecular charging and vibrational reorganization energies are demonstrated. By changing the resonance condition between the plasmon hybrid level and the molecular transition, a selective enhancement of different sections of the vibrational progression in the emission spectrum becomes possible. In any case, electroluminescence spectra are enlarged by more than three orders of magnitude.

PACS number(s): 85.65.+h, 78.60.Fi, 33.20.−t

I. INTRODUCTION

The capability of metal nanoparticles (MNPs) to enhance optical signals of nano-objects has led to outstanding scientific interest in their study (see Refs. 1–3 for a recent review). The orders-of-magnitude enhancement effect supports *single-molecule spectroscopy*, for example, the detection of photoemission spectra of an individual quantum dot or molecule. If the emitting state is prepared by nonoptical means, i.e., if single-molecule electroluminescence is considered as in Refs. 4–12, then such an enhancement is of particular interest. In a preliminary study, we suggested plasmon enhancement of molecular junction electroluminescence.[13] There, it has been assumed that the leads contacting the molecule form spherical MNPs with their hybridized dipole-plasmon excitations in resonance to the molecular optical transition.

In the following, we will present a detailed investigation of a modified system where two separate spherical MNPs sandwich the whole molecular junction (cf. Fig. 1). The leads shall be of pyramidal shape with plasmon resonances away from the molecular transition. The desired signal enhancement is achieved since the junction is placed into a MNP nanoresonator of a type as suggested, for example, in Refs. 14 and 15. By changing the resonator geometry, one can energetically tune the plasmon hybrid levels constituted by the coupled MNP excitations. Since this flexibility does not affect the molecular junction itself, it can work either in the direct or sequential regime of charge transmission. The sequential regime is of particular interest since an increasing residence time of the transmitted electron in the molecule increases the photoemission probability.

So far, electroluminescence according to the arrangement of Fig. 1 has not been realized in experiment. Instead, a scanning tunneling microscopy (STM) scheme with the molecules placed on a conducting layer and contacted by the STM tip were described (for example, Refs. 4–6). In these experiments, surface plasmons of the STM tip or the substrate are excited via inelastic electron tunneling (see also Ref. 16; the process is possible if the potential-energy difference between the molecule and STM tip is larger than surface-plasmon energy).

If the molecule is directly absorbed on the metal surface, the respective emission spectra are dominated by a broad plasmon emission line. This effect can be reduced by separating the molecules somewhat from the conducting layer. However, a pronounced plasmon enhancement was not observed.

Theoretical studies on single-molecule electroluminescence can be found in Refs. 9–12. These studies concentrate on the sequential regime of charge transmission and are in the position to offer emission spectra including the vibrational progression of a dominant molecular vibration. Alterations of this progression due to plasmon effects have also been reported in Refs. 10–12. However, only those plasmons were considered which were separately induced by electrons undergoing an inelastic tunneling process. They have been introduced into the description via a short external light pulse, but did not cause any emission enhancement. According to our subsequent discussion, this is due to the absence of any resonant molecule plasmon interaction. We will account for this coupling but ignore the tunneling-induced plasmon formation since the distance between the junctions and the MNP surfaces is larger than 1 nm (see also similar work in Refs. 17–19).

Consequently, it is the aim of the present investigations to demonstrate that the suggested scheme of Fig. 1 is ready to, first, realize direct and resonant molecule MNP-plasmon coupling and, second, to result in a remarkable enhancement of photoemission. The subsequent theory unifies our earlier work on molecular junctions[20–22] and on interacting molecule-MNP systems.[23–25]

Our description of sequential current formation in the molecular junction is summarized in Fig. 2. It focuses on charge transmission from the left to the right lead. In the considered sequential regime, charging appears via an incoherent transition of an electron from the left lead into the molecule. The energy of the charged molecule has to coincide with that of the neutral molecule plus the energy of a left-lead electron. As shown in the lower panel of Fig. 2, population of the excited electronic state of the charged molecule becomes possible at large applied voltages. Now, deexcitation of the molecule can also proceed as a radiative process just leading to molecular
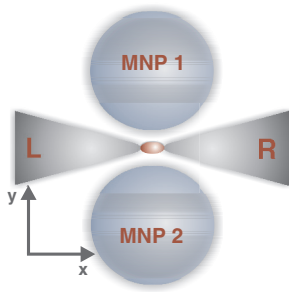
FIG. 1. (Color online) Planar arrangement of a molecular junction and two identical MNPs. The molecule (red) is contacted by a left (L) and a right (R) pyramidal electrode and sandwiched by two MNPs. The tip distance between the left and the right electrode is Δx and the minimal MNP-MNP surface distance (with the molecular center of mass in between) is $2\Delta y$. The scheme should correspond to Δx about 4 nm and $2\Delta y$ about 5 nm. The MNP diameter amounts to 20 nm (according to the tip shape, the lead-MNP distance is larger than 1 nm to avoid lead-MNP electron tunneling).

electroluminescence. Discharge of the molecule proceeds via the hop of the excess electron into an empty state; here, of the right lead. The middle panel of Fig. 2 displays a situation where the energy of the excited electronic state of the neutral molecule plus the energy of an empty electron level just above the Fermi sea of the right lead equal the ground-state energy of the charged molecule. Discharge realizes an excited-state population of the neutral molecule and, again, molecular electroluminescence becomes possible. If the molecular radiative transitions couple to MNP-plasmon excitations, an electroluminescence enhancement can be expected.

We describe this enhancement in a theory which considers the coupled molecule-MNP system as a uniform quantum system.[23–25] However, the present investigation will be restricted to singly excited states of the system (the presence of a molecular excitation, a single-plasmon excitation in one of the two MNPs, or a respective superposition state). The interaction between the molecule and the spherical MNPs appears as an energy exchange process including molecular electronic deexcitation and MNP-plasmon excitation (as well as the reverse process). This uniform treatment results in a direct description of Fano resonances and an enhancement of molecular quantities. Since in the present case the molecule is placed in a nanoresonator formed by two MNPs, the plasmon excitations hybridize. The resulting level splitting depends on the type of plasmon (polarization direction of the particular dipole plasmon; for details see below) and decreases with increasing distance between the two MNPs. Figure 3 displays the change of the different hybrid levels with inter-MNP distance. For the chosen molecular excitation energy, the resonance case can be achieved and particular large emission enhancement has to be expected.

The discussion of the MNP-enhanced single-molecule electroluminescence is organized as follows. In the next section, we introduce the used molecular junction nanoresonator model (the parameters that are used are discussed in Sec. IV). The applied density matrix theory is described in Sec. III, together with the formulas to compute the emission spectrum and the charge and energy current. A brief description of the
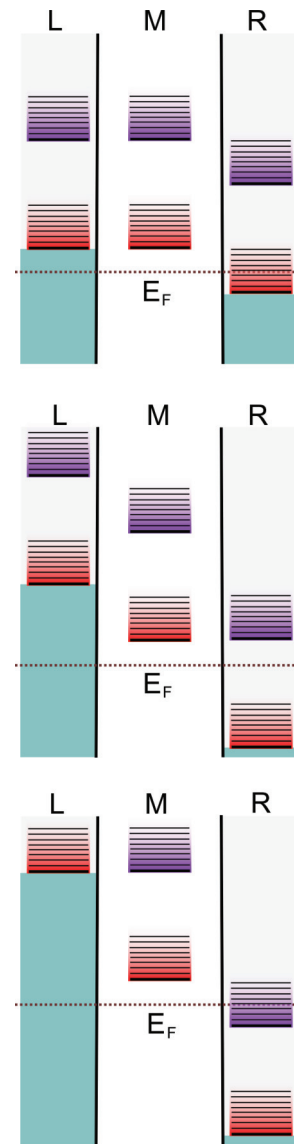
FIG. 2. (Color online) Energy-level scheme of the junction at three different applied voltages V. In the left lead L, the energies of the neutral molecule (thin lines indicate vibrational levels) are combined with the energy of an electron below or at the Fermi energy E_F (green region). For the right lead R, the energies of the neutral molecule are added to the energy of an electron above E_F (light-gray region). The central part M shows the energies of the singly charged molecule. The electronic ground-state vibrational energies are drawn with a red background and the excited-state vibrational energies are drawn with a purple background. The dotted line gives the position of E_F (at $V = 0$). Charging (from L to M) and discharging (from M to R) proceed as horizontal transitions. Upper panel: current formation starts via the electronic ground-state population of the charged molecule ($V = 2\Delta E_{10}/|e|$; for notation see Sec. IV). Middle panel: population of the neutral molecule's excited state sets in via discharge [$V = 2(E_{0eg} - \Delta E_{10})/|e|$]. Lower panel: population of the charged molecule's excited state becomes possible [$V = 2(E_{1eg} + \Delta E_{10})/|e|$].

junction properties in the absence of MNPs is offered in Sec. V. Section VI presents results on plasmon-enhanced electroluminescence. The paper ends with some concluding remarks in Sec. VII.
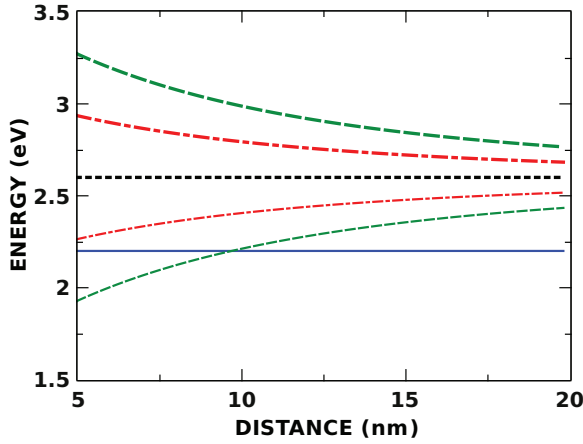
FIG. 3. (Color online) Nanoresonator plasmon hybrid levels $\mathcal{E}_{l\pm}$ vs MNP-MNP surface distance $2\Delta y$ (cf. Fig. 1). Red dash-dotted curves: $\mathcal{E}_{x\pm} = \mathcal{E}_{z\pm}$; green dashed curves: $\mathcal{E}_{y\pm}$; black dashed curve: single MNP dipole plasmon energy E_{pl}; blue solid curve: molecular excitation energy E_{eg}.

II. MODEL

The model corresponding to the molecular junction sandwiched between the two MNPs (see Fig. 1) has to account for the molecular energy levels at different charging states. Moreover, the properties of the leads as well as of the MNPs, including their coupling to the molecule, have to be considered and, finally, the continuum of photon states which are populated due to the radiative decay of the molecule and the MNPs shall also be included. Since the dynamics of charge transmission through the molecule is described using the density matrix theory (cf. Ref. 21), the whole model is constructed in the framework of open quantum system dynamics with the standard notation of the Hamiltonian: $H = H_{\mathrm{S}} + H_{\mathrm{R}} + H_{\mathrm{S-R}}$. The (primary) system Hamiltonian H_{S} covers the part of the system described explicitly, H_{R} characterizes the different types of reservoir, and $H_{\mathrm{S-R}}$ is the respective system-reservoir coupling. The system Hamiltonian takes the form

$$H_{\mathrm{S}} = H_{\mathrm{mol}} + H_{\mathrm{pl}} + H_{\mathrm{mol-pl}}. \quad (1)$$

The electron-vibrational states of the molecule at different charging are described by H_{mol}. Plasmon excitations of the two MNPs (and their hybridization) are accounted for by H_{pl}. Their coupling to molecular excitations is considered by $H_{\mathrm{mol-pl}}$.

These contributions have to be completed by different types of the reservoir (cf. also Fig. 4). Single electron-hole pair excitations in the MNP responsible for plasmon decay are considered as one type with Hamiltonian $H_{\mathrm{R}}^{(\mathrm{mnp})}$. Another type will be responsible for vibrational relaxation in the molecule. The related Hamiltonian of respective intramolecular vibrational energy redistribution (IVR) is $H_{\mathrm{R}}^{(\mathrm{IVR})}$. The Fermi sea of the two leads forms a third type of reservoir with Hamiltonian $H_{\mathrm{R}}^{(\mathrm{leads})}$ and, finally, transversal photon states constitute the fourth type of reservoir. The respective Hamiltonian is $H_{\mathrm{R}}^{(\mathrm{rad})}$. Accordingly, we obtain

$$H_{\mathrm{R}} = H_{\mathrm{R}}^{(\mathrm{mnp})} + H_{\mathrm{R}}^{(\mathrm{IVR})} + H_{\mathrm{R}}^{(\mathrm{leads})} + H_{\mathrm{R}}^{(\mathrm{rad})}. \quad (2)$$
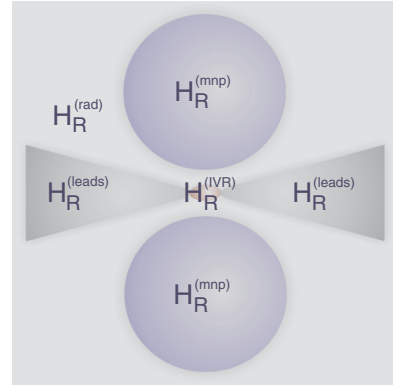
FIG. 4. (Color online) Different types of reservoir (R) with Hamiltonian H_{R} which have been introduced to describe electroluminescence of the molecular junction MNP system of Fig. 1. $H_{\mathrm{R}}^{(\mathrm{mnp})}$ refers to single electron-hole pair excitations in the MNPs responsible for plasmon decay. IVR processes in the molecule are accounted for by $H_{\mathrm{R}}^{(\mathrm{IVR})}$. Electrons of the left and right lead forming the current which passes through the molecule are considered by $H_{\mathrm{R}}^{(\mathrm{leads})}$. Transversal photon states populated in the emission process constitute $H_{\mathrm{R}}^{(\mathrm{rad})}$.

It results in a similar separation of the system-reservoir coupling,

$$H_{\mathrm{S-R}} = H_{\mathrm{S-R}}^{(\mathrm{mnp})} + H_{\mathrm{S-R}}^{(\mathrm{IVR})} + H_{\mathrm{S-R}}^{(\mathrm{leads})} + H_{\mathrm{S-R}}^{(\mathrm{rad})}. \quad (3)$$

The first part $H_{\mathrm{S-R}}^{(\mathrm{mnp})}$ describes the decay of collective MNP plasmon oscillations.[26–28] A coupling of the active molecular vibrations entering H_{mol} to the reservoir of secondary modes is incorporated in $H_{\mathrm{S-R}}^{(\mathrm{IVR})}$.[20,21] Electron exchange between the leads and the molecule is considered by $H_{\mathrm{S-R}}^{(\mathrm{leads})}$.[21] Finally, $H_{\mathrm{S-R}}^{(\mathrm{rad})}$ accounts for the radiative decay of molecular and plasmon excitations.[13,24,25] We consider $H_{\mathrm{S-R}}$ as a weak or moderate coupling and embed the whole description into standard density matrix theory (quantum master equation).[21,29]

All parts of the total Hamiltonian have already been described by us elsewhere. Therefore, we only briefly recapitulate the main expressions. We start with a presentation of the different parts of H_{S}. The molecular part is written as

$$H_{\mathrm{mol}} = \sum_{N,a,\mu} E_{Na\mu} |\Psi_{Na\mu}\rangle\langle\Psi_{Na\mu}|. \quad (4)$$

The quantum number N labels the number of excess electrons in the molecule, and a is the electronic quantum number covering the ground state ($a = g$) and the first excited state ($a = e$). Vibrational states are labeled by the quantum numbers μ. The molecular wave function $\Psi_{Na\mu}$ separates into the electronic part φ_{Na} and the vibrational part $\chi_{Na\mu}$. Often, a single high-frequency vibrational mode dominates the coupling to the molecular junction charge transmission.[31] Accordingly, the vibrational spectra are specified by the potential-energy surfaces (PES), $U_{Na}(Q) = U_{Na}^{(0)} + \hbar\omega_{\mathrm{vib}}(Q - Q_{Na})^2/4$ (Ref. 29; the vibrational energy quanta $\hbar\omega_{\mathrm{vib}}$ do not depend on the electronic states). The Q_{Na} are the electronic-state-dependent equilibrium values of Q, and $U_{Na}^{(0)} \equiv E_{Na}$ is the energy at the equilibrium configuration. Electronic transition energies E_{Neg} shall take the form $U_{Ne}^{(0)} - U_{Ng}^{(0)}$ and are assumed to be

independent of the charging state ($E_{Neg} = E_{eg}$). Reorganization energies related to intramolecular electronic transitions follow as $\lambda_{Ma,Nb} = \hbar\omega_{\text{vib}}/4 \times (Q_{Ma} - Q_{Nb})^2$. So, the overall energies take the form $E_{Na\mu} = E_{Na} + \mu\hbar\omega_{\text{vib}}$ (E_{Na} includes the vibrational zero-point energy.)

Plasmon excitations of the spherical MNPs (counted by m) can be restricted to dipole excitations. Those dominate the interaction with molecules (or other MNPs) provided the molecules are more than about 2 nm apart from the MNP surface.[23] As already indicated, we will limit the whole description to singly excited states of the molecular junction MNP system. Then, the related MNP Hamiltonian is restricted to single-plasmon excitations. Accordingly, the Hamiltonian of MNP $m = 1,2$ takes the form

$$H_{\text{pl}}^{(m)} = \hbar\Omega_{m0}|m0\rangle\langle m0| + \sum_I \hbar\Omega_{mI}|mI\rangle\langle mI|, \quad (5)$$

with the mth MNP ground state $|m0\rangle$ and the excited states $|mI\rangle$. The latter are threefold degenerated according to dipole-plasmon excitations with transition dipole moments pointing along the three axes of a Cartesian coordinate system. Therefore, we have $I = x,y,z$. To keep it simple, the two MNPs are assumed to be identical (i.e., the same metal and spherical shape with the same diameter). So, we set $\hbar(\Omega_{mI} - \Omega_{m0}) = E_{\text{pl}}$, where $E_{\text{pl}}/\hbar$ is the dipole-plasmon frequency.

In the presence of excited states, the Coulomb coupling between two MNPs (or between the molecule and a single MNP) is dominated by an energy-transfer interaction. If the interacting units (labeled by u and v) are positioned not too close to each other, the coupling can be taken in the approximation of interacting dipoles,

$$J_{uv} = \frac{[\mathbf{d}_u\mathbf{d}_v^*] - 3[\mathbf{d}_u\mathbf{n}][\mathbf{n}\mathbf{d}_v^*]}{|\mathbf{R}|^3}. \quad (6)$$

The $\mathbf{d}_u$ and $\mathbf{d}_v$ are the (transition) dipole moments, $\mathbf{R}$ is the vector connecting the center of mass of the two units, and $\mathbf{n}$ labels the respective unit vector $\mathbf{R}/|\mathbf{R}|$. In the case of the molecule, $\mathbf{d}_u$ can be identified with the electronic ground-state to excited-state transition dipole moment $\mathbf{d}_{\text{mol}}$ (a possible dependence on the charging state is ignored). Concerning the MNP, we have $\mathbf{d}_I = d_{\text{pl}}\mathbf{e}_I$ (the $\mathbf{e}_I$ with $I = x,y,z$ are unit vectors of a Cartesian coordinate system). The resulting molecule-MNP coupling can be written as

$$H_{\text{mol-pl}} = \sum_N \sum_{m,I} J_{N,mI}|\varphi_{Ne}\rangle\langle\varphi_{Ng}| \otimes |m0\rangle\langle mI| + \text{H.c.} \quad (7)$$

The inter-MNP coupling Hamiltonian looks similar, but with $J_{N,mI}$ replaced by $J_{m'I',mI}$ and $|\varphi_{Ne}\rangle\langle\varphi_{Ng}|$ replaced by $|m'I'\rangle\langle m'0|$. It completes $H_{\text{pl}}^{(1)} + H_{\text{pl}}^{(2)}$, given by Eq. (5), to result in the full expression for H_{pl}.

Having explained the active system, we turn to a description of the different types of reservoir Hamiltonian and related system-reservoir couplings. Concerning $H_{\text{R}}^{(\text{mnp})}$ and $H_{\text{S-R}}^{(\text{mnp})}$, we do not offer explicit expressions but refer to Refs. 26–28. The present approach is only affected by this type of reservoir via the dephasing rate of MNP dipole-plasmon states γ_{pl}.

Turning to vibrational relaxation (IVR), we will be a little bit more concrete and introduce (cf. also Refs. 21 and 22)

$$H_{\text{S-R}}^{(\text{IVR})} = \sum_{N,a,\xi} \hbar k_\xi(Na)(Q - Q_{Na})Z_\xi|\varphi_{Na}\rangle\langle\varphi_{Na}|. \quad (8)$$

This type of system-reservoir coupling [with coupling coefficients $k_\xi(Na)$] represents a bilinear coupling between the single active and dimensionless vibrational coordinate Q and a reservoir of secondary vibrations with coordinates Z_ξ. These modes should undergo harmonic vibrations (the Hamiltonian is $H_{\text{R}}^{(\text{IVR})}$).

The third type of reservoir is given by the Fermi sea of left- and right-lead electrons. The related system-reservoir coupling is responsible for molecular charging and discharging[20,21] and takes the form

$$\begin{aligned}
H_{\text{S-R}}^{(\text{leads})} &= \sum_{N,a,b} \sum_{X,\mathbf{k},s} V_X(N+1a,Nb;\mathbf{k})a_{X\mathbf{k}s}|\varphi_{N+1a}\rangle\langle\varphi_{Nb}| \\
&+ \sum_{N,a,b} \sum_{X,\mathbf{k},s} V_X(N-1a,Nb;\mathbf{k})a_{X\mathbf{k}s}^\dagger|\varphi_{N-1a}\rangle\langle\varphi_{Nb}|.
\end{aligned} \quad (9)$$

The operator $a_{X\mathbf{k}s}^\dagger$ creates an electron in lead $X = L,R$ with wave vector $\mathbf{k}$ and spin s, while $a_{X\mathbf{k}s}$ annihilates the respective electron (wave vectors of bulk metal electrons are only of symbolic value and have to be replaced by concrete quantum numbers valid for the pyramidal leads). The related energies are $\epsilon_{X\mathbf{k}}$. Together with the creation and annihilation operators, they constitute $H_{\text{R}}^{(\text{leads})} = \sum_{X,\mathbf{k},s} \epsilon_{X\mathbf{k}}a_{X\mathbf{k}s}^\dagger a_{X\mathbf{k}s}$. The matrix elements $V_X(N+1a,Nb;\mathbf{k})$ entering $H_{\text{S-R}}^{(\text{leads})}$ describe molecular charging (from level b to level a) and the $V_X(N-1a,Nb;\mathbf{k})$ are responsible for molecular discharge (for more details, see Refs. 20 and 21).

The remaining coupling to the reservoir of transversal photons is written as[24]

$$H_{\text{S-R}}^{(\text{rad})} = \hbar\sum_{\lambda,\mathbf{k}} \hat{h}_{\lambda\mathbf{k}}(b_{\lambda\mathbf{k}} + b_{\lambda\mathbf{k}}^\dagger). \quad (10)$$

The $b_{\lambda\mathbf{k}}^\dagger$ and $b_{\lambda\mathbf{k}}$ are the creation and annihilation operators of photons, respectively, with polarization λ, wave vector $\mathbf{k}$, and energy $\hbar\omega_{\mathbf{k}}$ [the resulting photon Hamiltonian $H_{\text{R}}^{(\text{rad})}$ takes the standard form $\sum_{\lambda,\mathbf{k}} \hbar\omega_{\mathbf{k}}(b_{\lambda\mathbf{k}}^\dagger b_{\lambda\mathbf{k}} + 1/2)$]. The coupling operator $\hat{h}_{\lambda\mathbf{k}}$ can be presented in a compact form if we introduce A as the quantum number of molecular excited states ($A = Ne$) and of the MNP's excited states ($A = mI$):

$$\hat{h}_{\lambda\mathbf{k}} = \sum_A g_{\lambda\mathbf{k}}(A)|\phi_A\rangle\langle\phi_g| + \text{H.c.} \quad (11)$$

In the case of the coupling to molecular excitations, the transition operator is $|\varphi_{Ne}\rangle\langle\varphi_{Ng}|$ and the coupling constant reads $g_{\lambda\mathbf{k}}(Ne) = -i\sqrt{2\pi E_{eg}^2/V\hbar^3\omega_{\mathbf{k}}} \times [\mathbf{n}_{\lambda\mathbf{k}}\mathbf{d}_{\text{mol}}]$ (we introduced the quantization volume V, and $\mathbf{n}_{\lambda\mathbf{k}}$ is the unit vector of transversal photon polarization). Turning to the coupling to MNP plasmons, the transition operator takes the form $|mI\rangle\langle m0|$ and we have $g_{\lambda\mathbf{k}}(mI) = -i\sqrt{2\pi E_{\text{pl}}^2/V\hbar^3\omega_{\mathbf{k}}} \times [\mathbf{n}_{\lambda\mathbf{k}}\mathbf{d}_{mI}]$.

III. DENSITY MATRIX THEORY

The tackled system-reservoir description of electroluminescence requires the introduction of the reduced density operator $\hat{\rho}(t)$. It is defined as the trace of the total statistical operator $\hat{W}(t)$ with respect to the reservoir states, i.e., $\hat{\rho}(t) = \text{tr}_R\{\hat{W}(t)\}$. The standard quantum master equation for $\hat{\rho}(t)$ which we only have in mind here is obtained by a second-order approximation with respect to H_{S-R} (see, for example, Ref. 29).

The choice of the states used to introduce the density matrix determines which type of excitation of the molecular junction MNP system is considered. Since we will concentrate on the low-excitation regime, we restrict the description to a single excitation in the system. This might be either a molecular excitation or a single-plasmon excitation of one of the MNPs. Of course, a superposition state of such states is also allowed. But higher excited states, for example, a double or triple excitation of MNP dipole plasmons, should be very unlikely. Consequently, we consider product states of the molecule (two) MNP system of the type

$$|Ne\mu,00\rangle = |\Psi_{Ne\mu}\rangle|m=1,0\rangle|m=2,0\rangle. \quad (12)$$

Here, the excitation is localized at the molecule (both MNPs remain unexcited). The other type of excited states reads

$$|Ng\nu,I0\rangle = |\Psi_{Ng\nu}\rangle|m=1,I\rangle|m=2,0\rangle, \quad (13)$$

or

$$|Ng\nu,0I\rangle = |\Psi_{Ng\nu}\rangle|m=1,0\rangle|m=2,I\rangle. \quad (14)$$

The excitation is localized at one of the two MNPs. The state of the unexcited system (however, including possible vibrational excitations) is

$$|Ng\nu,00\rangle = |\Psi_{Ng\nu}\rangle|m=1,0\rangle|m=2,0\rangle. \quad (15)$$

All of these states will be abbreviated by $|\alpha\rangle$. The Hamiltonian resulting from an expansion of H_S, given by Eq. (1), is introduced in Appendix A, and the density matrix reads $\rho_{\alpha\beta}(t) = \langle\alpha|\hat{\rho}(t)|\beta\rangle$. The related equations of motion are taken in a form where the dissipative part does not couple diagonal and off-diagonal elements of the density matrix,[30]

$$\frac{\partial}{\partial t}\rho_{\alpha\beta} = -\frac{i}{\hbar}\tilde{\varepsilon}_{\alpha\beta}\rho_{\alpha\beta} - \frac{i}{\hbar}\sum_\gamma(V_{\alpha\gamma}\rho_{\gamma\beta} - \rho_{\alpha\gamma}V_{\gamma\beta})$$
$$-\delta_{\alpha,\beta}\sum_\gamma(k_{\alpha\to\gamma}\rho_{\alpha\alpha} - k_{\gamma\to\alpha}\rho_{\gamma\gamma}). \quad (16)$$

The complex transition energies are defined as $\tilde{\varepsilon}_{\alpha\beta} = \varepsilon_{\alpha\beta} - i(1-\delta_{\alpha,\beta})\hbar\gamma_{\alpha\beta}$, where $\varepsilon_{\alpha\beta} = \varepsilon_\alpha - \varepsilon_\beta$ is determined by the energies ε_α of the ground and the singly excited states of the molecule-MNP system (see Appendix A). Dephasing is accounted for by

$$\gamma_{\alpha\beta} = \frac{1}{2}\sum_\gamma(k_{\alpha\to\gamma} + k_{\beta\to\gamma}) + \delta_{M,N}\delta_{\mu,0}\delta_{\nu,0}\gamma^{(\text{pd})}. \quad (17)$$

The dephasing rates include transition rates $k_{\alpha\to\beta}$ and, if necessary, pure dephasing rates $\gamma^{(\text{pd})}$.

A. Transition rates

In the most general approach, the $k_{\alpha\to\beta}$ can be formulated without a perturbational expansion with respect to the

molecule-MNP and to the inter-MNP energy-transfer coupling (cf., e.g., Ref. 29). Here, we calculate all rates in zeroth order with respect to these couplings (see the discussion below). There are four types of transition rates:

$$k_{\alpha\to\beta} = k_{\alpha\to\beta}^{(\text{non-rad})} + k_{\alpha\to\beta}^{(\text{IVR})} + k_{\alpha\to\beta}^{(\text{leads})} + k_{\alpha\to\beta}^{(\text{rad})}. \quad (18)$$

They are related to the four types of a reservoir introduced in Eq. (2). The rate of nonradiative decay describes the finite plasmon lifetime.[23] It should be diagonal with respect to the charging number (and only exist for the molecular ground state). If the MNP $m=1$ is concerned, we have

$$k_{Ng\mu,I0\to Ng\nu,00}^{(\text{non-rad})} = \delta_{\mu,\nu}2\gamma_{\text{pl}}. \quad (19)$$

In general, the initial state of the considered transition depends on the molecular charging and on the particular dipole plasmon excited in one of the MNPs. Since we assume a uniform plasmon damping, the concrete rate expression considers that identical molecular vibrational levels are only involved. The rate $k_{Ng\mu,0I\to Ng\nu,00}^{(\text{non-rad})}$ describing decay of the second MNP has the same form.

The IVR rate is obtained from the coupling expression given by Eq. (8).[20–22] It is diagonal with respect to the charging number and the molecular electronic level,

$$k_{Na\mu,00\to Na\nu,00}^{(\text{IVR})} = J_{Na}(\omega_{\text{vib}})\{\delta_{\nu,\mu+1}(\mu+1)n(\omega_{\text{vib}}) + \delta_{\nu,\mu-1}\mu[1+n(\omega_{\text{vib}})]\}. \quad (20)$$

Here, $n(\omega_{\text{vib}})$ is the Bose-Einstein distribution function and $J_{Na}(\omega_{\text{vib}})$ denotes the spectral density of the coupling of the primary mode to the reservoir of secondary modes. Note that the particular rate $k_{Ng\mu,00\to Ng\nu,00}^{(\text{IVR})}$ (molecular ground-state to ground-state transition) is identical with those where one MNP is excited.

The rates $k_{\alpha\to\beta}^{(\text{leads})}$ are caused by the coupling of the molecule to the two leads.[20–22] The molecular charging rate is (general transition energies have been reduced to the molecular part)

$$k_{N-1a\mu,00\to Nb\nu,00}^{(\text{leads})}$$
$$= \sum_X \Gamma_{N-1a,Nb}^{(X)}(E_{Nb\nu,N-1a\mu})$$
$$\times |\langle\chi_{N-1a\mu}|\chi_{Nb\nu}\rangle|^2 f_F(E_{Nb\nu,N-1a\mu} - \mu_X)$$
$$= \sum_X k_{N-1a\mu\to Nb\nu}^{(X)}, \quad (21)$$

and that responsible for discharge reads

$$k_{N+1a\mu,00\to Nb\nu,00}^{(\text{leads})}$$
$$= \sum_X \Gamma_{N+1a,Nb}^{(X)}(E_{N+1a\mu,Nb\nu})|\langle\chi_{N+1a\mu}|\chi_{Nb\nu}\rangle|^2$$
$$\times [1 - f_F(E_{N+1a\mu,Nb\nu} - \mu_X)]$$
$$= \sum_X k_{N+1a\mu\to Nb\nu}^{(X)}. \quad (22)$$

The rates $k_{N\pm1g\mu,00\to Ng\nu,00}^{(\text{leads})}$ (molecular ground-state to ground-state transition) are completed by those where one MNP is in its excited state. The above given formulas contain the Fermi function $f_F(E)$, the chemical potential μ_X of lead X, as well as the vibrational overlap expression $\langle\chi_{N\pm1a\mu}|\chi_{Nb\nu}\rangle$.

The remaining expression $\Gamma^{(X)}_{N\pm1a,Nb}(E)$ is the molecule-lead coupling function, which takes the form

$$\Gamma^{(X)}_{N\pm1a,Nb}(E) = \frac{2\pi}{\hbar} \sum_{\mathbf{k},s} |V_X(N\pm1a,Nb,\mathbf{k})|^2 \delta(E - \varepsilon_{X\mathbf{k}}).$$

(23)

In the so–called wide band limit, it reduces to a constant.

Finally, we present the rates of radiative decay. They have been discussed at length in Ref. 24, including the molecule-MNP energy-transfer coupling. This introduces a certain enhancement of the radiative decay rate of the molecule, but is of minor importance for the overall kinetics (the molecular radiative lifetime is reduced from a value in the ns region to a value of some hundreds of ps). The only important term is the MNP radiative decay rate, which may reach about 30% of the nonradiative rate $2\gamma_{\text{pl}}$. Because of this, we ignore the inter-MNP coupling and use[24]

$$k^{(\text{rad})}_{Ng\mu,I0\to Ng\mu,00} = \frac{4\omega^3_{\text{pl}}}{3c^3\hbar} |d_{\text{pl}}|^2.$$

(24)

The expression is diagonal in the molecular quantum numbers, and the other rate $k^{(\text{rad})}_{Ng\mu,0I\to Ng\mu,00}$ looks similar. Both rates appear as a simplified version of the frequency integrated emission spectrum, which is introduced in the subsequent section.

B. The emission spectrum

The frequency-resolved emission spectrum $F(\omega)$ has been derived at several places (cf. Ref. 24 and references therein). A brief derivation can be found in Appendix B. One obtains

$$F(\omega) = \frac{4\omega^3}{3\pi c^3\hbar} \text{Re} \int_0^\infty dt\, e^{-i\omega t}$$
$$\times \sum_{N,A,B} [\mathbf{d}_A \mathbf{d}_B^*] \sum_{\mu,\nu} \langle \chi_{NA\nu} | \chi_{Ng\mu,00} \rangle$$
$$\times \sum_{C,\kappa} \sigma_{Ng\mu,00;NC\kappa}(t;NB) \rho_{NC\kappa,NA\nu}. \quad (25)$$

The quantity $F(\omega)$ is the probability of photon emission per frequency (it covers all polarizations and spatial directions, thus it is not angle resolved). If integrated with respect to ω, it results in the radiative lifetime of the coupled molecule-MNP complex. To achieve a sufficiently compact notation of $F(\omega)$, the new quantum number A labels excited electronic states of the system, i.e., $\alpha = Ne\mu,00 = NA\mu$ as well as $Ng\mu,I0 = NA\mu$ and $Ng\mu,0I = NA\mu$ (if the ground state is concerned, we further write $Ng\mu,00$). Accordingly, $\chi_{NA\nu}$ might be $\chi_{Ne\nu}$ but also $\chi_{Ng\nu}$ if A refers to an excited MNP state. Since A refers to product states of the system and the charging number N is quoted explicitly, A differs from the quantum numbers introduced in relation to Eq. (11).

The density matrix elements $\rho_{NC\kappa,NA\mu}$ appearing in Eq. (25) account for the actual steady state of the coupled molecular junction MNP system. The newly defined density matrix follows as

$$\sigma_{Ng\mu,00;NC\kappa}(t;NB) = \langle Ng\mu,00 | \hat{\sigma}(t;NB) | NC\kappa \rangle, \quad (26)$$

with the operator $\hat{\sigma}(t;NB) = \mathcal{U}(t)|Ng,00\rangle\langle NB|$. The time-evolution superoperator $\mathcal{U}(t)$ generates the equation of motion

for the reduced density operator. The state $|Ng,00\rangle$ is the electronic part of the system ground state and $|NB\rangle$ is the electronic part of $|NB\nu\rangle$. Accordingly, the initial condition for σ is $\sigma_{Ng\mu,00;NC\kappa}(t=0;NB) = \langle Ng\mu,00|Ng,00\rangle\langle NB|NC\kappa\rangle$ (for more details, see Appendix B). Then, Fourier transformation of the σ functions results in the frequency dependence of the emission spectrum, given by Eq. (25). The combination of dipole moments characterizing either the molecular excitation or the MNP-plasmon excitations guarantees plasmon hybrid-level formation as well as Fano-like structures in the emission.

C. Charge and energy currents

The presented rates for molecular charging and discharging constitute the formula for the current moving from lead X into the molecule,[21]

$$I_X = |e| \sum_\alpha k_{\alpha\to X} \rho_{\alpha\alpha}. \quad (27)$$

The rates

$$k_{Na\mu\to X} = \sum_{b,\nu} \left(k^{(X)}_{Na\mu\to N+1b\nu} - k^{(X)}_{Na\mu\to N-1b\nu} \right) \quad (28)$$

are determined by the rates introduced in Eqs. (21) and (22).

Besides the electric current, we consider energy flow through the molecule by computing the change of the active system energy $E_S = \text{tr}_S\{\hat{\rho}(t)H_S\}$ with time. Noting the equation of motion for $\hat{\rho}$ and the approximation of the dissipative part $-\mathcal{D}\hat{\rho}$ as taken in Eq. (16), we get (cf. also Ref. 29)

$$\frac{\partial}{\partial t} E_S = -\text{tr}_S\{H_S \mathcal{D}\hat{\rho}(t)\}$$
$$= -\sum_{\alpha,\beta} \varepsilon_{\alpha\beta} k_{\alpha\to\beta} \rho_{\alpha\alpha} - \sum_{\alpha,\beta}(1-\delta_{\alpha,\beta})\gamma_{\alpha\beta}\rho_{\alpha\beta}V_{\beta\alpha}. \quad (29)$$

The first term on the right-hand side can be rewritten as $\sum_{\alpha,\beta}\rho_{\alpha\alpha}k_{\alpha\to\beta}\varepsilon_{\beta\alpha}$. Here, $\varepsilon_{\beta\alpha}$ gives the energy change due to the particular $\alpha \to \beta$ transition. The total energy gain (or loss) per time follows by weighting all transitions with the transition probabilities $\rho_{\alpha\alpha}k_{\alpha\to\beta}$. Coupling energies among different states are considered in the second term on the right-hand side of Eq. (29) (our numerical computations indicate that this term is small and can be ignored).

According to the separation of the transition rates, given by Eq. (18), into four different contributions, we can split $\partial E_S/\partial t$ into

$$\frac{\partial}{\partial t} E_S = R^{(\text{non-rad})} + R^{(\text{IVR})} + R^{(\text{leads})} + R^{(\text{rad})}. \quad (30)$$

In the steady state, $\partial E_S/\partial t = 0$, energy outflow from the molecule due to electronic and vibrational relaxation, i.e., $R^{(\text{non-rad})} + R^{(\text{IVR})} + R^{(\text{rad})}$, is balanced by energy input $R^{(\text{leads})}$ due to charge transmission through the molecule.

IV. THE MOLECULAR JUNCTION MNP SYSTEM

In carrying out experiments on single-molecule electroluminescence, different types of molecules have been used so far.[32] Accordingly, a parameterized model is introduced in the present study to cover the variety of these molecules and also to investigate different energetic configurations of the molecular junction MNP system. The introduced parameters can be found

TABLE I. Parameters used in this study (for explanation, see text).

ΔE_{10}	0.05–1 eV
E_{eg}	1.925 eV
$\hbar\omega_{\mathrm{vib}}$	50 meV
Q_{0g}	0
Q_{0e}	2
Q_{1g}	3
Q_{1e}	1
d_{mol}	8 D
$\hbar\gamma_{\mathrm{mol}}$	3 meV
$\hbar J$	1 meV
$\hbar\Gamma$	1 meV
r_{mnp}	10 nm
E_{pl}	2.6 eV
d_{pl}	2893 D
$\hbar\gamma_{\mathrm{pl}}$	28.5 meV
$k_{\mathrm{B}}T$	5 meV

in Table I and are in line with our preliminary investigation of Ref. 13.

In contrast to Ref. 13, however, we consider pyramidal leads and two separate spherical MNPs which form a nanoresonator and establish hybrid levels (cf. Sec. VI). The MNPs are given by Au nanoparticles with a diameter of 20 nm and with a dipole-plasmon excitation energy around 2.6 eV (concerning the lifetime broadening γ_{pl} and the transition dipole moment d_{pl}; see also Table I).

As in our earlier studies, we again focus on a molecular junction which operates in the regime of sequential charge transmission (this is also in line with the experiments of Ref. 6). According to this case of weak molecule-lead electron transfer coupling, the related coupling parameter Γ is small (the given value of Table I has to be considered as an upper limit in this respect). Since our focus is not on specific molecule-lead coupling effects, we use a common quantity which is identical for the two leads and all involved electronic levels. Moreover, we assume that in the considered voltage range, only the singly negatively charged state of the molecule participates in the current formation. The molecular electronic energies are E_{Na} (see Sec. II; possible electrostatic couplings of the charged molecule to the leads and the MNPs shall be included in the definition of the energies E_{1a}). The difference $\Delta E_{10} = E_{1g} - E_{0g} - \mu_0$ gives the so-called *relative charging energy* (μ_0 is the uniform chemical potential of the leads). Since less is known about ΔE_{10}, we consider it as a parameter and set $\Delta E_{10} > 0$, i.e., charging is impossible in the absence of an applied voltage. The additional assumptions, $E_{2g} - E_{1g} \gg \mu_0$ and $E_{0g} - E_{-1g} \ll \mu_0$, guarantee that double charging and hole transfer, respectively, do not contribute for all applied voltages. Figure 2 displays possible processes of molecular charging and discharging as analyzed in the following. The model of a symmetrically applied voltage is used by replacing the actual Fermi energy of the left lead by $E_{\mathrm{F}} + |e|V/2$ and that of the right lead by $E_{\mathrm{F}} - |e|V/2$.

As already indicated in Sec. II, we will concentrate on a model with a single active vibrational coordinate. This is confirmed by experiments which indicate the dominance of one vibrational mode when charging or discharging of the molecule (different types of a copper phthalocyanine) takes place.[31] The vibrational energy $\hbar\omega_{\mathrm{vib}}$ has been taken in a form independent of the electronic state and shall amount to 50 meV. Reorganization energies $\lambda_{Ma,Nb}$ may refer to charging ($M = 1, N = 0$) or to molecular excitation ($M = N, a = e, b = g$). To have a noticeable nuclear rearrangement upon charging, we set $\lambda_{1g,0g} = 112.5$ meV, while the $\lambda_{0e,0g}$ and $\lambda_{1e,1g}$ related to electronic transition are 50 meV. In the course of discussing the results, these values following from Table I will be changed also. IVR as introduced in Eq. (20) is determined by the single value $J = J_{Na}(\omega_{\mathrm{vib}})$ of a common spectral density (cf. Table I; it results in a lifetime $1/J$ of the first excited vibrational state of about 0.5 ps).

V. ABSENCE OF MNP PLASMON EFFECTS

In order to highlight below the effect of molecule-MNP coupling, we first briefly consider the case where this coupling is absent. The behavior of the steady-state current versus applied voltage is well documented in the literature (for an overview, see Refs. 34–37). Here, we mainly focus on the contributions of molecular excited electronic states. Figure 5 displays the IV characteristics at different reorganization energies $f\lambda_{Ma,Nb}$. The values $\lambda_{Ma,Nb}$ correspond to the parameters given in Table I and $f = 4, 2.25, 1, 0.25, 0$ scales down the reorganization energy up to a vanishing electron-vibrational coupling ($f = 0$; the different f values are realized by a proper change of the Q_{Ma}).

The behavior of the IV curves is easily understood in using the energy scheme of Fig. 2 (note the small value of 50 meV for the relative charging energy ΔE_{10} and also remember the additional assumption $E_{1eg} = E_{0eg} \equiv E_{eg}$). The background curve of Fig. 5, corresponding to the case of vanishing electron-vibrational coupling, displays three plateaus. The current starts to move if the applied voltage is large enough to realize conditions as drawn in the upper part of Fig. 2. The energy of the neutral molecule (in its electronic ground state) combined with the actual Fermi energy of the left lead coincides with the energy of the charged molecule: $E_{0g} + E_{\mathrm{F}} + eV/2 = E_{1g}$ (be aware of the absence of vibrational contributions). It results
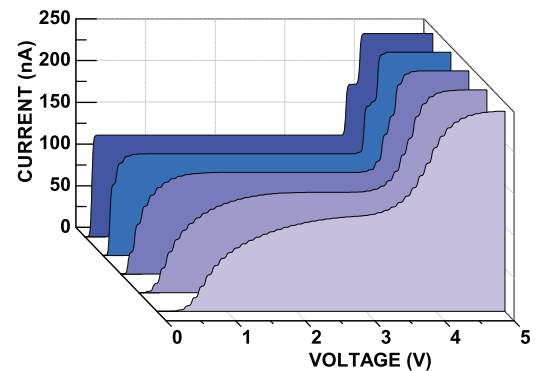
FIG. 5. (Color online) IV characteristics of the molecular junction at different reorganization energies $\lambda_{Ma,Nb}$ (absence of molecule-MNP coupling). Curve in the center is with parameters according to Table I. Other curves with $\lambda_{Ma,Nb}$ changed by the prefactor $f = 0, 0.25, 1, 2.25, 4$ (from background to foreground).

in $eV = 2\Delta E_{10}$, i.e., the current from the left to the right lead starts to flow at 0.1 V. The involved charge motion from the molecule to the right lead is also possible since the right lead offers energies of empty electron levels $F_{el} > E_F - eV/2$ which, if combined with E_{0g}, realize molecular discharge.

The described charge transmission regime does not change up to a voltage, which results in the energy-level scheme of the middle panel of Fig. 2. Now, discharge of the molecule becomes also possible via a population of the excited electronic state: $E_{1g} = E_{eg} + E_{0g} + E_F - eV/2$. A new channel for charge transmission has been open [at $eV = 2(E_{eg} - \Delta E_{10})$] and the steady-state current moves to a second plateau. The last plateau in the background curve of Fig. 5 is reached if the electronically excited state of the charged molecule is populated. The lower panel of Fig. 2 indicates that $E_{0g} + E_F + eV/2$ (see left lead) has to coincide with $E_{1e} = E_{eg} + E_{1g}$. So, the last current plateau starts at $V = 2(E_{eg} + \Delta E_{10})/e$.

The second and the third plateaus in the IV characteristics correspond to the molecular excited-state population. Therefore, we expect the appearance of electroluminescence in this voltage range. However, the large voltage values up to 5 V would be critical for the junction stability (as explained later, the voltage range can be noticeably reduced when using molecules leading to a larger relative charging energy). When increasing the molecular reorganization energies, additional small steps due to the participation of vibrational levels appear and the second current plateau vanishes. Moreover, the current sets in at larger voltages when the reorganization energies are increased. This reflects the well-known phenomenon of the so-called Franck-Condon blockade.

Total steady-state populations $P_{Na} = \sum_\mu \rho_{Na\mu,Na\mu}$ of the molecular electronic levels for the case of the reference reorganization energies (values according to Table I) are displayed in Fig. 6. In line with the foregoing description of the IV characteristics, excited states are empty in the voltage range below 3.6 V and $P_{0g} \approx P_{1g} \approx 0.5$ is realized. Increasing further the applied voltage, excited molecular states are populated. Finally, the case $P_{Na} = 0.25$ is reached, indicating that noticeable photon emission becomes possible. A typical
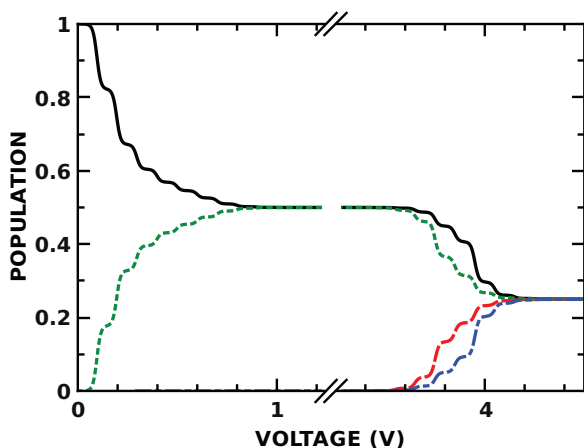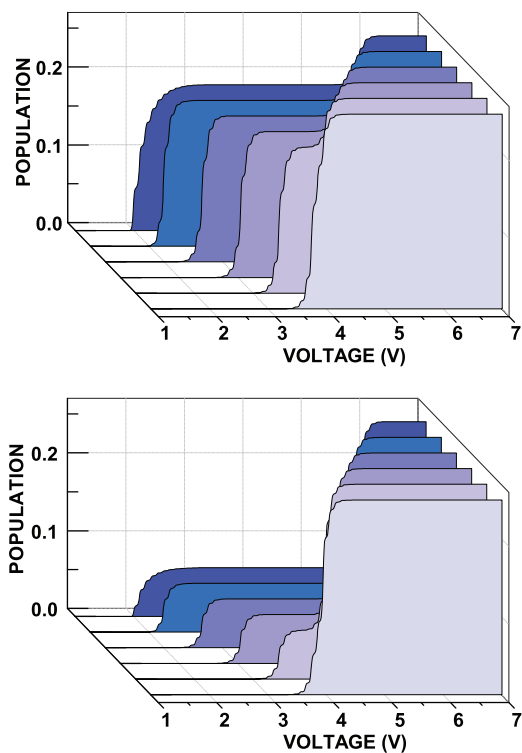
FIG. 7. (Color online) Steady-state populations P_{Ne} of excited molecular states (parameters according to Table I; absence of molecule-MNP coupling). Variation of the relative charging energy ΔE_{10}. From foreground to background: $\Delta E_{10} = 0.05, 0.2, 0.4, 0.6, 0.8, 1$ eV. Upper panel: P_{0e}. Lower panel: P_{1e}.

emission spectrum (without plasmon enhancement) is shown in Fig. 9 (foremost red filled curve, applied voltage 4.2 V). According to the chosen reorganization energies, a noticeable broad vibrational progression appears (curve increased by a factor of 1000).

As already indicated, a decrease of the voltage range where electroluminescence has to be expected can be achieved by changing to molecules with a larger relative charging energy ΔE_{10}. Figure 7 shows the steady-state populations P_{Ne} of the excited molecular states with ΔE_{10} increasing up to 1 eV. Having a molecule with $\Delta E_{10} > 0.6$ eV electroluminescence shall already appear in the 2 V region.

As a final discussion in this section, we consider the energy balance in the junction (without coupling to the MNP). In the steady state, the energy per time $R^{(leads)}$ put into the molecule via the coupling to the leads is nearly identical to the vibrational energy per time $-R^{(IVR)}$ dissipated via relaxation [cf. Eq. (30); radiative decays are of minor importance]. Figure 8 displays $R^{(leads)} \approx -R^{(IVR)}$ versus the applied voltage and for different IVR rates. If IVR is nearly absent, then $R^{(leads)}$ is small since almost no energy is dissipated in the molecule. The work necessary to be done at the molecule via charge injection and charge outflow increases with increasing IVR strength. It also increases with increasing voltage up to the range where the excited-state population starts (cf. Fig. 5). This increase is caused by the population of higher-lying vibrational levels (in the molecular electronic ground state) which goes along with an enlarged amount of vibrational energy dissipated via IVR (see also Fig. 2). If excited electronic states become populated,

FIG. 6. (Color online) Total steady-state populations P_{Na} of the molecular electronic levels (parameters according to Table I; absence of molecule-MNP coupling). Black solid line: P_{0g}; green dotted line: P_{1g}; red dashed line: P_{0e}; blue dashed dotted line: P_{1e}.
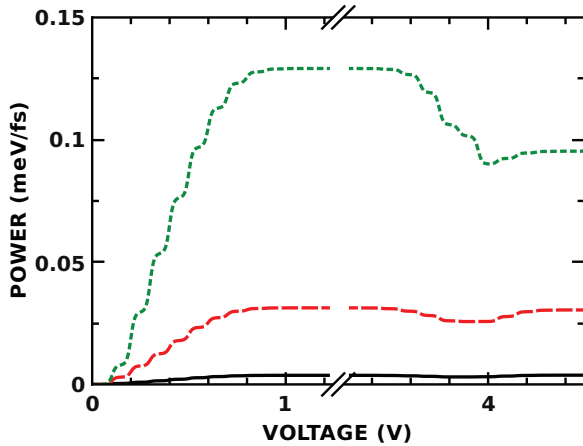
FIG. 8. (Color online) Steady-state energy balance of the molecular junction in the absence of the MNPs. Shown is the energy per time $R^{\text{(leads)}}$ put into the molecule via the coupling to the leads [note $R^{\text{(leads)}} \approx -R^{\text{(IVR)}}$]. Variation of IVR strength (other parameters according to Table I). Black solid curve: $\hbar J = 0.01$ meV; red dashed curve: $\hbar J = 0.1$ meV; green dotted curve: $\hbar J = 1$ meV.

then the respective low-lying excited vibrational states are also occupied, which reduces the amount of dissipated energy.

VI. PRESENCE OF MNP PLASMON EFFECTS

After the brief consideration of what has to be expected if MNP-plasmon effects are absent, we study in the following the electroluminescence of the molecular junction embedded in the MNP nanoresonator (cf. Fig. 1). In order to interpret the emission spectra, we introduce the MNP hybrid levels which did not appear in the description so far (the applied density matrix is based on single MNP excited states as well as their coupling, accounting in this way for hybrid-level formation indirectly). Noting the MNP-MNP surface distance $2\Delta y > 5$ nm (remember the symmetric arrangement of Fig. 1), the coupling is dominated by a dipole-plasmon–dipole-plasmon interaction, given by Eq. (6). Among the various matrix elements $J_{m'I',mI}$, nonzero terms are $J_{1x,2x} = J_{1z,2z} = J_{\text{pl}}$ and $J_{1y,2y} = -2J_{\text{pl}}$ (interchange of $m' = 1$ and $m = 2$ is also possible). Note that $J_{\text{pl}} = d_{\text{pl}}^2/(2R_{\text{mol}-\text{mnp}})^3$, where $R_{\text{mol}-\text{mnp}} = \Delta y + r_{\text{mnp}}$ is the center-to-center distance between the molecule and one of the MNPs. The decoupling of the plasmon excitations with respect to the three Cartesian coordinate indices $I = x,y,z$ simply results in the six hybrid levels $\mathcal{E}_{x\pm} = \mathcal{E}_{z\pm} = E_{\text{pl}} \pm J_{\text{pl}}$ and $\mathcal{E}_{y\pm} = E_{\text{pl}} \pm 2J_{\text{pl}}$. Figure 3 shows the respective energies versus the MNP-MNP surface distance Δy (cf. Fig. 1). To realize the resonance case between $\mathcal{E}_{y-}$ and the molecular excitation energy E_{eg}, we took the latter somewhat larger as in Table I (see also below).

The following discussion of electroluminescence focuses on the effect due to the actually applied voltage. We also display results caused by a detuning of the hybrid levels with respect to the molecular excitation energy (via changing the MNP-MNP distance). The effect due to a change of the molecular transition dipole moment orientation and due to a change of the molecular reorganization energies is also discussed.
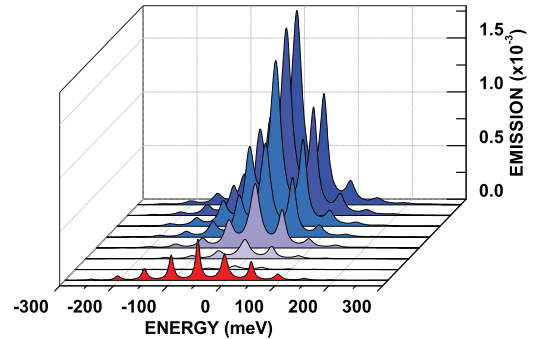
FIG. 9. (Color online) Steady-state emission spectra of the molecular junction coupled to the nanoresonator vs photon energy (relative to the molecular excitation energy E_{eg}; parameters according to Table I; MNP-MNP surface distance $2\Delta y = 5$ nm; $\mathbf{d}_{\text{mol}} || \mathbf{e}_y$, cf. Fig. 1). Variation of the applied voltage. From background to foreground: $V = 4.2, 4.1, 4.0, 3.9, 3.8, 3.7, 3.6$ V (cf. Fig. 5). The foremost red filled curve shows the emission for a molecular junction decoupled from the MNPs (increased by 1000; applied voltage 4.2 V).

A. Change of the applied voltage

We consider the case of a small relative charging energy (cf. Table I) and vary the applied voltage in the range where excited molecular states become populated. According to Fig. 6, this covers the voltage range between 3 and 4 V. Figure 9 offers respective emission spectra. At the chosen MNP-MNP distance, the molecular excitation energy $E_{eg} = 1.925$ eV is in resonance to $\mathcal{E}_{y-}$. This hybrid level is of interest since the molecular transition dipole moment has been assumed to point in the y direction (cf. Fig. 1). Accordingly, a strong enhancement of the emission spectrum around the photon energy of $\hbar\omega = E_{eg}$ appears. To rationalize this, note the respective emission spectrum in the absence of a molecule-MNP coupling (foremost red filled curve in Fig. 9). The chosen reorganization energies result in a rather broad vibrational progression. Since it also corresponds to the case of 4.2 V, we can state a more-than-three order-of-magnitude plasmon enhancement of the molecular junction's electroluminescence (the red filled curve has to be compared with the backmost blue filled curve).

B. Change of the MNP-MNP distance

Changing the MNP-MNP distance changes the energetic position of the plasmon hybrid levels. We take a somewhat higher molecular excitation energy compared to Table I and move $\mathcal{E}_{y-}$ through E_{eg} when varying $2\Delta y$ between 5 and 16 nm (see Fig. 3). Figure 10 shows how the increasing hybrid plasmon energy (what is caused by an increase of $2\Delta y$) results in the enhancement of different parts of the molecular emission spectrum. As long as $\mathcal{E}_{y-} < E_{eg}$ ($2\Delta y < 10$ nm), a separate plasmon resonance becomes visible and the low part of the vibrational progression is strongly enhanced and deformed. The decreasing intensity which goes along with the increase of $\mathcal{E}_{y-}$ is originated by an increasing detuning and a decreasing molecule-MNP coupling with increasing distance.

In the right panel of Fig. 10, we confronted these results with those obtained for a molecule with very small (vanishing) reorganization energies. The molecular emission is
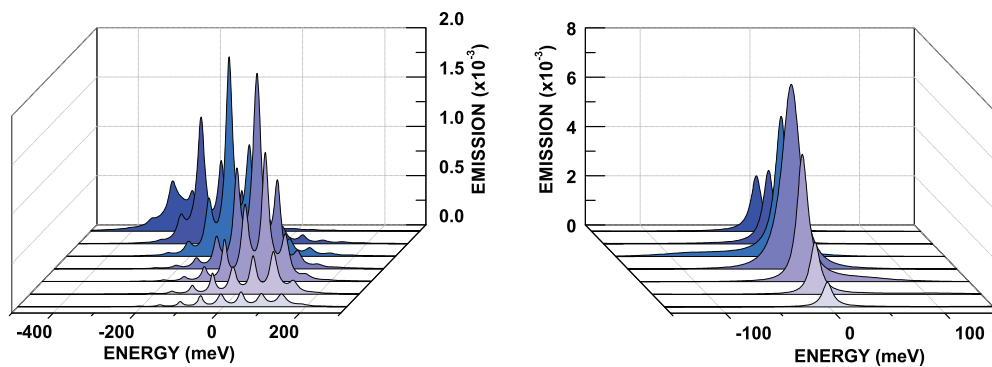
FIG. 10. (Color online) Steady-state emission spectra of the molecular junction coupled to the nanoresonator vs photon energy (relative to the molecular excitation energy $E_{eg} = 2.2$ eV; other parameters according to Table I; applied voltage 4.8 V; $\mathbf{d}_{\mathrm{mol}}||\mathbf{e}_y$, cf. Fig. 1). Variation of plasmon hybrid-level position via a variation of the MNP-MNP surface distance $2\Delta y = 5, 6, 8, 10, 12, 14, 16$ nm (from background to foreground; cf. Fig. 3). Left panel: reorganization energies according to Table I. Right panel: absence of electron-vibrational coupling (vanishing reorganization energies).

characterized by a single peak which increases with decreasing detuning between $\mathcal{E}_{y-}$ and E_{eg}. The third curve from the back ($2\Delta y = 8$ nm), where $\mathcal{E}_{y-} < E_{eg}$, displays a small structure at the low-energy shoulder of the main peak. It belongs to the hybrid plasmon level (cf. also the discussion in Ref. 13). So, if detuning is present, the molecule strongly couples to the MNPs, but an enhancement of the sole molecular emission takes place. In contrast, the curve for $2\Delta y = 10$ nm combines the molecular and MNP emission in one line.

C. Change of the molecular transition dipole moment orientation

Emission spectra for different orientations of the molecular transition dipole moment $\mathbf{d}_{\mathrm{mol}}$ are shown in Fig. 11. In order to demonstrate that all three MNP hybrid levels can be addressed by choosing appropriate spatial orientations of $\mathbf{d}_{\mathrm{mol}}$, the molecular excitation energy E_{eg} has been placed at 2.47 eV. Taking $2\Delta y = 8$ nm, we arrive at $\mathcal{E}_{y-} < E_{eg} < \mathcal{E}_{x+}, \mathcal{E}_{z+}$ (the MNP hybrid levels are off-resonant to the molecular excitation). A coupling to the hybrid level $\mathcal{E}_{y-}$ is achieved
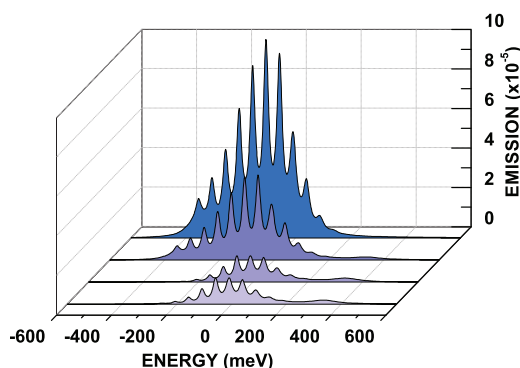
FIG. 11. (Color online) Steady-state emission spectra of the molecular junction coupled to the nanoresonator vs photon energy (relative to the molecular excitation energy $E_{eg} = 2.47$ eV; other parameters according to Table I; applied voltage 5 V; MNP-MNP surface distance $2\Delta y = 8$ nm). Different orientations of the molecular transition dipole moment $\mathbf{d}_{\mathrm{mol}}$ (cf. Fig. 1). From background to foreground: $\mathbf{d}_{\mathrm{mol}}||\mathbf{e}_y, \mathbf{d}_{\mathrm{mol}}||\mathbf{e}_x + \mathbf{e}_y + \mathbf{e}_z, \mathbf{d}_{\mathrm{mol}}||\mathbf{e}_x, \mathbf{d}_{\mathrm{mol}}||\mathbf{e}_z$.

if $\mathbf{d}_{\mathrm{mol}} || \mathbf{e}_y$, and a coupling to $\mathcal{E}_{x+}$ ($\mathcal{E}_{z+}$) becomes possible if $\mathbf{d}_{\mathrm{mol}} || \mathbf{e}_x$ ($\mathbf{d}_{\mathrm{mol}} || \mathbf{e}_z$). If we set $\mathbf{d}_{\mathrm{mol}} || \mathbf{e}_x + \mathbf{e}_y + \mathbf{e}_z$, however, all hybrid levels are addressed. Comparing these spectra with those in the absence of the molecule-MNP coupling (not shown), the spectrum for $\mathbf{d}_{\mathrm{mol}} || \mathbf{e}_y$ is about 500 times larger, the spectrum for $\mathbf{d}_{\mathrm{mol}} || \mathbf{e}_x$ ($\mathbf{d}_{\mathrm{mol}} || \mathbf{e}_z$) displays an enhancement by 100 times, and that for $\mathbf{d}_{\mathrm{mol}} || \mathbf{e}_x + \mathbf{e}_y + \mathbf{e}_z$ by 200 times.

The enhancement effect for $\mathbf{d}_{\mathrm{mol}} || \mathbf{e}_y$ is the largest one since the total MNP dipole-plasmon populations,

$$P_1 = \sum_{N,\mu,I} \rho_{Ng\mu,I0;Ng\mu,I0}, \qquad (31)$$

and

$$P_2 = \sum_{N,\mu,I} \rho_{Ng\mu,0I;Ng\mu,0I}, \qquad (32)$$

amount to $P_1 = P_2 = 4.4 \times 10^{-4}$. If $\mathbf{d}_{\mathrm{mol}} || \mathbf{e}_x, \mathbf{e}_z$, then the population only reaches the value of 5.7×10^{-5}.

D. Change of the molecular reorganization energies

Figure 12 displays a situation where E_{eg} is in near resonance to $\mathcal{E}_{y-}$ ($\mathbf{d}_{\mathrm{mol}}||\mathbf{e}_y$; $2\Delta y = 5$ nm). The reorganization energies $\lambda_{Ma,Nb}$ have been varied as in Sec. V and Fig. 5. The separation of a single line at $\lambda_{Ma,Nb} = 0$ into a widened vibrational progression along with decreasing emission line intensities becomes visible.

E. Energy balance

Finally, we discuss the change of the energy flow through the molecule if it is coupled to the two MNPs. Figure 13, upper panel, displays a slight decrease of the steady-state current. This behavior can be interpreted as a resistance increase due to an increased energy dissipation by the molecule and the MNPs (plasmon decay, IVR, photon emission). Such an enlarged dissipation becomes more obvious in the lower panel of Fig. 13, where the energy per time $R^{(\mathrm{leads})}$ transmitted into the molecule via the coupling to the leads is shown. Moving the applied voltage into the range where the excited level of the molecule (either being in its neutral or charged state) becomes populated (cf. Fig. 6), $R^{(\mathrm{leads})}$ increases strongly. Here, the red
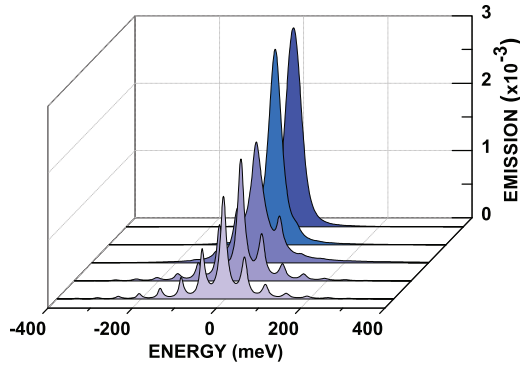
FIG. 12. (Color online) Steady-state emission spectra of the molecular junction coupled to the nanoresonator vs photon energy (relative to the molecular excitation energy $E_{eg} = 1.925$ eV; other parameters according to Table I; applied voltage 4.4 V; MNP-MNP surface distance $2\Delta y = 5$ nm; $\mathbf{d}_{mol} || \mathbf{e}_y$, cf. Fig. 1). Variation of molecular reorganization energies $\lambda_{Ma,Nb}$ by the prefactor $f = 0, 0.25, 1, 2.25, 4$ (from background to foreground).

dashed curve has to be confronted with the black one, which is identical to the green dotted curve of Fig. 8 (i.e., absence of the molecule-MNP coupling). This increase of $R^{(\text{leads})}$ reflects
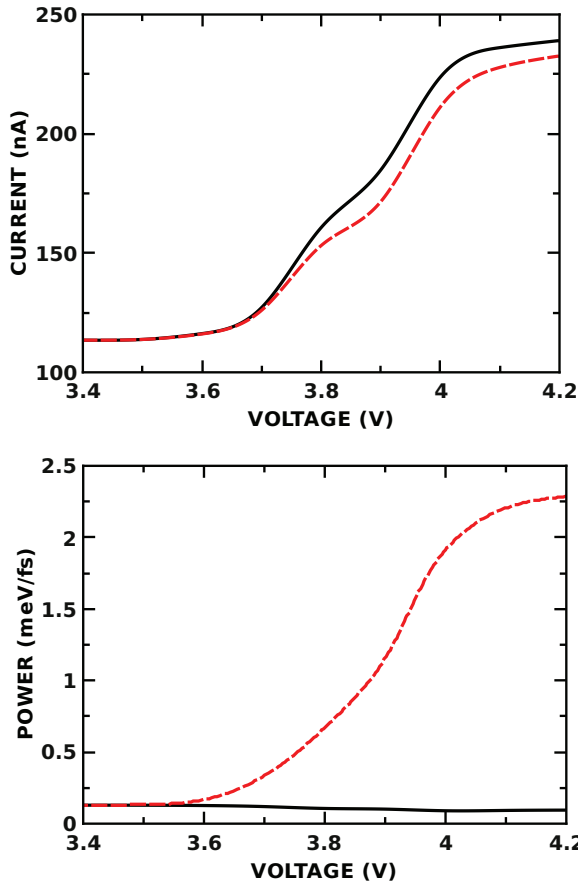
FIG. 13. (Color online) IV characteristics and steady-state energy balance for the molecular junction coupled to the nanoresonator (red dashed curves) and decoupled from it (black solid curves; use of the same parameters as in green dashed curve of Fig. 8). Upper panel: IV characteristics. Lower panel: energy per time $R^{(\text{leads})}$ transmitted into the molecule via the coupling to the leads.
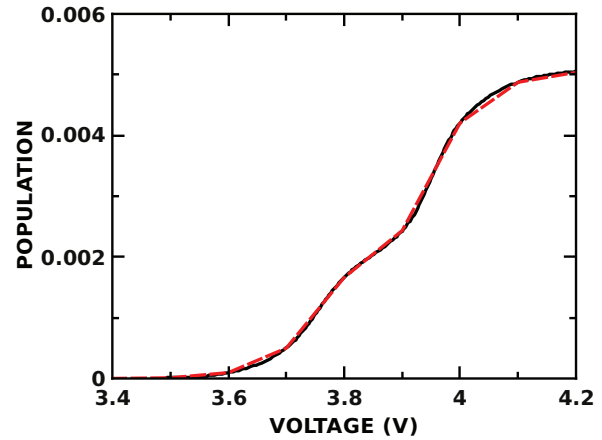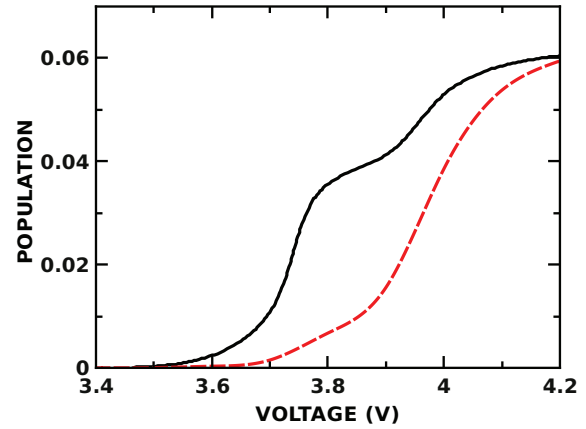
FIG. 14. (Color online) Steady-state populations of the excited molecular levels P_{0e}, P_{1e} and of the total MNP plasmon excitations $P_{m=1,2}$, given by Eqs. (31) and (32) (same parameters as in Fig. 9). Upper panel: black solid curve denotes P_{0e}; red dashed curve denotes P_{1e}. Lower panel: black solid curve denotes $P_{m=1}$; red dashed curve denotes $P_{m=2}$.

the onset of the coupling to the MNP hybrid level. If the levels are populated, a fast energy dissipation starts due to the short plasmon lifetime. The increase of $R^{(\text{leads})}$ also covers the enlarged portion of energy per time which is dissipated due to an enhanced photon emission rate.

Figure 14 indicates that the molecule-MNP coupling goes along with a strong decrease of the excited-state population P_{0e} (molecule in its neutral state) and P_{1e} (molecule in its singly charged state). Noting these quantities in the absence of the molecule-MNP coupling as drawn in Fig. 6, a nearly one order-of-magnitude decrease becomes obvious. At the same time, a steady-state dipole plasmon population in the per mill range appears. These small excited-state populations of the molecule-MNP system prove that the restriction on singly excited states, as done in the formulation of the general approach, is sufficient for the chosen parameter range (and multiple excited states are of no importance).

VII. CONCLUSIONS

In continuing earlier investigations of Ref. 13, electroluminescence of a molecular junction placed in a nanoresonator,

which is formed by two Au spheres, has been studied theoretically. The computations are based on a density matrix approach valid for the regime of sequential charge transmission through the molecule. An enhancement of the related photoemission by more than three orders of magnitude could be demonstrated. The surface plasmon excitation is caused by excitation energy-transfer coupling between the excited molecule and the hybrid plasmon levels. This mechanism is different from MNP-plasmon excitations due to the inelastic electron tunneling process as described in Ref. 16. The simulations also account for nonradiative and radiative decay as well as vibrational relaxation. In changing the distance between the two spheres, the hybrid plasmon levels formed by the nanoresonator can be varied and possibly be moved into resonance to the molecular transition. A selective enhancement of different parts of the vibrational progression in the emission spectrum becomes possible. So, the whole molecular spectrum can be scanned by changing the MNP-MNP distance. Molecules with a charging energy (relative to the lead's Fermi energy) in the 1 eV range allow for electroluminescence enhancement at an applied bias around 2 to 3 V. Considering the energy balance of the molecular junction nanoresonator system, the plasmon excitation, photoemission enhancement, and nonradiative plasmon decay could be related to an increased energy put into the molecule via its coupling to the leads.

The given considerations focus on a singly excited state of the coupled molecule nanoresonator system. If the molecule-lead coupling is large enough, the fast population of excited molecular states may pump multiple plasmon excitations of the MNPs[38] (plasmon lifetime may be increased by changing to those of doped graphene). This also requires a sufficiently strong molecule-MNP coupling. Accordingly, the molecular emission in the presence of multiple plasmon excitations should be further increased. This mechanism is the subject of ongoing work.

ACKNOWLEDGMENTS

APPENDIX A: LOW-EXCITATION HAMILTONIAN

To reduce the description of the molecular junction MNP system to only singly excited states besides the ground state, we introduced in Sec. III the states $|\alpha\rangle$, given by Eqs. (12)–(15). An expansion of the active-system Hamiltonian, given by Eq. (1), simply reads

$$H_{\mathrm{S}} = \sum_{\alpha,\beta} H_{\alpha\beta} |\alpha\rangle\langle\beta|, \tag{A1}$$

with the Hamiltonian matrix $H_{\alpha\beta} = \delta_{\alpha,\beta}\varepsilon_\alpha + (1 - \delta_{\alpha,\beta})V_{\alpha\beta}$. According to the definition of the quantum number α, there appear the energies $\varepsilon_{Ng\mu,00}$, $\varepsilon_{Ne\mu,00}$, $\varepsilon_{Ng\mu,I0}$, and $\varepsilon_{Ng\mu,0I}$. The overall ground-state energy takes the form

$$\varepsilon_{Ng\mu,00} = E_{Ng\mu} + \hbar(\Omega_{10} + \Omega_{20}) = E_{N0} + \mu\hbar\omega_{\mathrm{vib}}. \tag{A2}$$

E_{N0} is the total electronic ground-state energy (including vibrational zero-point energy) and $\mu\hbar\omega_{\mathrm{vib}}$ is the related

vibrational excitation energy. The energy of the molecular excitation is written as

$$\varepsilon_{Ne\mu,00} = E_{Neg} + \mu\hbar\omega_{\mathrm{vib}} + E_{N0}, \tag{A3}$$

where the molecular excitation energy $E_{Neg} = E_{Ne\mu=0} - E_{Ng\mu=0}$ has been introduced. If one MNP is excited (here with $m = 1$), we get the energy

$$\varepsilon_{Ng\mu,I0} = \hbar(\Omega_{1I} - \Omega_{10}) + \mu\hbar\omega_{\mathrm{vib}} + E_{N0}. \tag{A4}$$

The off-diagonal elements $V_{\alpha\beta}$ of the Hamiltonian matrix $H_{\alpha\beta}$ cover molecule-MNP interaction via $V(Ne\mu,00|Ng\nu,I0)$ and $V(Ne\mu,00|Ng\nu,0I)$ (coupling to the first and the second MNP, respectively), and the inter-MNP coupling $V(Ng\mu,I0|Ng\nu,0I')$. Noting Eqs. (6) and (7) for the coupling, we get, for example,

$$V(Ne\mu,00|Ng\nu,I0) = \langle\chi_{Ne\mu}|\chi_{Ng\nu}\rangle J_{N,1I}. \tag{A5}$$

The coupling $J_{N,1I}$ responsible for energy transfer from the first MNP ($m = 1$) to the molecule is weighted by a vibrational overlap expression. Furthermore, we have

$$V(Ng\mu,I0|Ng\nu,0I') = \delta_{\mu,\nu} J_{1I,2I'}. \tag{A6}$$

Of course, there are also complex conjugated versions of the considered coupling matrix elements.

APPENDIX B: SPONTANEOUS EMISSION OF THE MOLECULAR JUNCTION MNP SYSTEM

The computation of the photon emission rate $R_{\lambda\mathbf{k}}(t)$ is based on a second-order perturbation theory with respect to $H_{\mathrm{S-R}}^{(\mathrm{rad})}$, given by Eq. (10). As done earlier (see Ref. 24 and references therein), $R_{\lambda\mathbf{k}}(t) \equiv R_\lambda(\omega,t)$ can be determined as the time derivative of the photon-number expectation value. Then, the spontaneous emission rate as the number of photons emitted per frequency interval and at time t reads

$$F(\omega,t) = \frac{V\omega^2}{(2\pi c)^3} \sum_\lambda \int do\, R_\lambda(\omega,t), \tag{B1}$$

where $\int do$ abbreviates solid angle integration and V is the quantization volume. The second-order expression for the photon emission rate is

$$R_{\lambda\mathbf{k}}(t) = 2\mathrm{Re} \int_{t_0}^t d\bar{t}\, e^{-i\omega_{\mathbf{k}}(t-\bar{t})} \mathrm{tr}_{\mathrm{S}}\{\hat{h}_{\lambda\mathbf{k}}[\mathcal{U}(t-\bar{t})\hat{h}_{\lambda\mathbf{k}}\hat{\rho}(\bar{t})]\}. \tag{B2}$$

The coupling operators $\hat{h}_{\lambda\mathbf{k}}$ have been introduced in Eq. (11), and $\mathcal{U}$ is the time-evolution superoperator which generates the equation of motion for the density operator $\hat{\rho}$. Next, we insert the concrete form of $\hat{h}_{\lambda\mathbf{k}}$ and neglect off-resonant contributions. Noting also the restriction to singly excited states only, the emission rate can be written as (A and B label excited electronic states)

$$R_{\lambda\mathbf{k}}(t) = 2\mathrm{Re} \int_{t_0}^t d\bar{t}\, e^{-i\omega_{\mathbf{k}}(t-\bar{t})} \sum_{N,A,A'} g_{\lambda\mathbf{k}}(NA)g_{\lambda\mathbf{k}}^*(NA')$$
$$\times \mathrm{tr}_{\mathrm{vib}}\{\langle Ng,00|[\mathcal{U}(t-\bar{t})|Ng,00\rangle\langle NB|\hat{\rho}(\bar{t})]|NA\rangle\}. \tag{B3}$$

The used states are the electronic part of the electron-vibrational states introduced in Eqs. (12)–(15). The latter are considered via the vibrational-state trace.

Next, one changes to $F(\omega,t)$, given by Eq. (B1), and takes into consideration the concrete form of the coupling constants $g_{\lambda\mathbf{k}}(NA)$. This allows one to profit from the identity

$$\sum_\lambda \int do \big[\mathbf{d}_A \mathbf{n}_{\lambda\mathbf{k}} \big] \big[\mathbf{n}_{\lambda\mathbf{k}} \mathbf{d}_{A'}^* \big] = \frac{8\pi}{3} \big[\mathbf{d}_A \mathbf{d}_{A'}^* \big], \qquad (B4)$$

where $\mathbf{d}_A$ abbreviates the involved transition dipole moments. In a final step, to arrive at Eq. (25), one replaces the vibrational trace by introducing vibrational states suitable for the actual electronic states and takes the density operator $\hat{\rho}$ in Eq. (B3) at the actual time t, which is appropriate for the steady state. In the limit $t - t_0 \to \infty$, we arrive at $F(\omega)$, given by Eq. (25).

---

*may@physik.hu-berlin.de

[1] N. J. Halas, Nano Lett. **10**, 3816 (2010).

[2] T. W. Odom and G. C. Schatz, Chem. Rev. **11**, 3667 (2011).

[3] M. S. Tame, K. R. McEnery, S. K. Özdemir, J. Lee, S. A. Maier, and M. S. Kim, Nat. Phys. **9**, 329 (2013).

[4] X. H. Qiu, G. V. Nazin, and W. Ho, Science **299**, 542 (2003).

[5] Z. C. Dong, X. L. Guo, A. S. Trifonov, P. S. Dorozhkin, K. Miki, K. Kimura, S. Yokoyama, and S. Mashiko, Phys. Rev. Lett. **92**, 086801 (2004).

[6] S. W. Wu, G. V. Nazin, and W. Ho, Phys. Rev. B **77**, 205430 (2008).

[7] C. Zhang, R. Zhang, S. Jiang, L. Zhang, H. Y. Gao, X. L. Zhang, L. G. Chen, Y. Liao, and Z. C. Dong, Appl. Phys. Lett. **100**, 073111 (2012).

[8] N. L. Schneider and R. Berndt, Phys. Rev. B **86**, 035445 (2012).

[9] J. S. Seldenthuis, H. S. J. van der Zant, M. A. Ratner, and J. M. Thijssen, Phys. Rev. B **81**, 205430 (2010).

[10] G. Tian, J. C. Liu, and Y. Luo, Phys. Rev. Lett. **106**, 177401 (2011).

[11] G. Tian and Y. Luo, Phys. Rev. B **84**, 205419 (2011).

[12] G. Tian and Y. Luo, Angew. Chem. Int. Ed. **52**, 1 (2013).

[13] Y. Zhang, Y. Zelinskyy, and V. May, J. Phys. Chem. C **116**, 25962 (2012).

[14] A. Bek, R. Jansen, M. Ringler, S. Mayilo, T. A. Klar, and J. Feldmann, Nano Lett. **8**, 485 (2008).

[15] M. Ringler, A. Schwemer, M. Wunderlich, A. Nichtl, K. Kürzinger, T. A. Klar, and J. Feldmann, Phys. Rev. Lett. **100**, 203002 (2008).

[16] B. N. J. Persson and A. Baratoff, Phys. Rev. Lett. **68**, 3224 (1992).

[17] M. Sukharev and M. Galperin, Phys. Rev. B **81**, 165307 (2010).

[18] B. D. Fainberg, M. Sukharev, T. H. Park, and M. Galperin, Phys. Rev. B **83**, 205425 (2011).

[19] A. J. White, B. D. Fainberg, and M. Galperin, J. Phys. Chem. Lett. **3**, 2738 (2012).

[20] V. May and O. Kühn, Phys. Rev. B **77**, 115439 (2008).

[21] L. Wang and V. May, Chem. Phys. **375**, 252 (2010).

[22] L. Wang and V. May, PhysChemChemPhys **13**, 8755 (2011).

[23] Y. Zelinskyy, Y. Zhang, and V. May, J. Phys. Chem. A **116**, 11330 (2012).

[24] Y. Zhang, Y. Zelinskyy, and V. May, J. Nanophot. **6**, 063533 (2012).

[25] Y. Zelinskyy and V. May, Nano Lett. **12**, 446 (2012).

[26] L. G. Gerchikov, C. Guet, and A. N. Ipatov, Phys. Rev. A **66**, 053202 (2002).

[27] G. Weick, R. A. Molina, D. Weinmann, and R. A. Jalabert, Phys. Rev. B **72**, 115410 (2005).

[28] G. Weick, G.-L. Ingold, R. A. Jalabert, and D. Weinmann, Phys. Rev. B **74**, 165421 (2006).

[29] V. May and O. Kühn, *Charge and Energy Transfer Dynamics in Molecular Systems* (Wiley-VCH, Weinheim, 2000).

[30] When ignoring the coupling between diagonal and off-diagonal density matrix elements induced by the dissipative part (Redfield tensor), relaxation and dephasing in the system under consideration are somewhat approximated.[29] Phenomena such as coherence-induced population formation and population-induced coherence transfer are neglected. Moreover, dissipation has not been formulated with the eigenstates of the coupled molecule-MNP system. The Redfield tensor is of zero order with respect to the energy exchange coupling given by Eq. (6). In the present case, however, all of these approximations only slightly alter the central effect of MNP-plasmon-enhanced photoemission. The essential coherence between the molecular and the MNP excitation is not governed by the dissipative, but by the reversible, part of the density matrix equation. In addition, transition-rate-determined population redistribution and coherence dephasing are fully considered. There is also a particular effect due to that part of the overall Redfield tensor which follows from the electron transfer coupling between the molecule and the leads. It may induce coherences between different charging states of the molecule.[21] This is also of no interest for the present investigation and also requires a model with more charged states than the single one considered here.

[31] X. H. Qiu, G. V. Nazin, and W. Ho, Phys. Rev. Lett. **92**, 206102 (2004).

[32] Molecular junctions with tetraphenyl porphyrins were described in Refs. 7,8, and 10 and measurements on junctions with magnesium porphine were reported in Ref. 6. The experiments of Ref. 33 have been based on ethyne-bridged (porphinato) zinc(II) oligomers and, in Ref. 15, emitted photons of the fluorescence dye 2.5 Cy3 could be detected. Related basic electronic excitation energies extend from about 1.5 eV (Refs. 6 and 33) up to 1.9 eV.[7,8,10]

[33] P. Banerjee, D. Conklin, S. Nanayakkara, T. H. Park, M. J. Therein, and D. A. Bonnell, ACS Nano **4**, 1019 (2010).

[34] G. Cuniberti, G. Fagas, and K. Richter, *Introducing Molecular Electronics*, Lecture Notes in Physics Vol. 680 (Springer, Berlin, Heidelberg, 2005), pp. 1-10.

[35] M. Galperin, M. A. Ratner, and A. Nitzan, J. Phys.: Condens. Matter **19**, 103201 (2007).

[36] J. Cueva and E. Scheer, *Molecular Electronics: An Introduction to Theory and Experiment* (World Scientific, Singapore, 2010).

[37] N. A. Zimbovskaya and M. R. Perderson, Phys. Rep. **509**, 1 (2011).

[38] A. Manjavacas, P. Nordlander, and F. Javier Garcia de Abajo, ACS Nano **6**, 1724 (2012).